

# Journal of Materials Chemistry C

Accepted Manuscript



This is an *Accepted Manuscript*, which has been through the Royal Society of Chemistry peer review process and has been accepted for publication.

*Accepted Manuscripts* are published online shortly after acceptance, before technical editing, formatting and proof reading. Using this free service, authors can make their results available to the community, in citable form, before we publish the edited article. We will replace this *Accepted Manuscript* with the edited and formatted *Advance Article* as soon as it is available.

You can find more information about *Accepted Manuscripts* in the [Information for Authors](#).

Please note that technical editing may introduce minor changes to the text and/or graphics, which may alter content. The journal's standard [Terms & Conditions](#) and the [Ethical guidelines](#) still apply. In no event shall the Royal Society of Chemistry be held responsible for any errors or omissions in this *Accepted Manuscript* or any consequences arising from the use of any information it contains.

Cite this: DOI: 10.1039/c0xx00000x

www.rsc.org/xxxxxx

ARTICLE TYPE

# Substitution Degree Engineering the Crystal Packing and Optoelectronic Properties of Benzofuranvinyl-Substituted Benzene-Cored Derivatives

Jin-Xing Qiu,<sup>a</sup> Ye-Xin Li,<sup>\*a,b</sup> Xiao-Feng Yang,<sup>a</sup> Yong Nie,<sup>a</sup> Zhen-Wei Zhang,<sup>a</sup> Zhong-He Chen,<sup>a</sup> and Guo-Xin Sun<sup>\*a</sup>

Received (in XXX, XXX) Xth XXXXXXXXX 20XX, Accepted Xth XXXXXXXXX 20XX

DOI: 10.1039/b000000x

In order to explore new furan-based functional materials, investigate the effect of multi-branched degree on the optoelectronic properties and search for three-dimensional organic semiconductors from planar  $\pi$ -conjugated molecules, compounds 1,4-bis[2-(benzofuran-2-yl)vinyl]benzene (**2BFVB**) with linear shape, 1,3,5-tris[2-(benzofuran-2-yl)vinyl]benzene (**3BFVB**) with star shape and 1,2,4,5-tetra[2-(benzofuran-2-yl)vinyl]benzene (**4BFVB**) with cruciform shape were synthesized and compared. **2BFVB** adopt a two-dimensional herringbone packing motif and there are two kinds of molecule conformations. The crystal packing of **3BFVB** is more sensitive to the crystallization condition. Two single-crystal phases and one thin-film phase were found. **3BFVB** ( $\beta$ -phase) molecules pack into a three-dimensional cofacial herringbone structure. **4BFVB** forms an inter-inserted two-dimensional hexagon packing. The molecular shape and aggregate packing exert remarkable effects on the optoelectronic properties. The quantum yield of **2BFVB** is very high both in the solution (74%) and in the crystalline solid (76%) state. The high solid emission efficiency of **2BFVB** is possibly related to the two molecule conformations in the herringbone-arranged H-aggregates. Both **2BFVB** and **3BFVB** display hole-transport ability. The performance of **3BFVB** amorphous film is nearly equal to that of its crystalline film, which would be helpful to simplify the device fabrication. This study shows that the substitution degree exerts drastic effects on the solubility, polymorphism, crystal packing and optoelectronic properties.

## Introduction

In these years, great process has been made in the device performance and the fabrication technique of organic field-effect transistors (OFETs).<sup>1</sup> The organic semiconductor layer is a key component in the OFET device, and the solid molecule packing plays an important role in the carrier-transport ability. The crystal structures of inorganic semiconductors usually have high symmetry and the carrier transport possesses a three-dimensional (3D) feature. In contrary, except to a rather few examples such as C<sub>60</sub>, most organic  $\pi$ -conjugated molecules have low symmetry and aggregate into solid with columnar or lamellar structure by van der Waals force. Organic molecules usually interact strongly in one or several directions but weakly in the other directions, bearing a typical anisotropic feature. Therefore, organic  $\pi$ -conjugated materials usually belong to one (1D) or two (2D)-dimensional semiconductor. Organic materials with a 3D electronic structure are very limited.<sup>2</sup> Theoretical calculations have showed that, considering the structural disorder, the dimensionality of the charge percolation network can exert a drastic influence on the carrier mobility. Organic charge transporting materials with a 2D or 3D network are more advantageous than 1D semiconductors.<sup>3</sup> In search of the organic

silicon, molecules with a 3D geometry such as tetrahedral system with a silicon, nitrogen or sp<sup>3</sup> carbon centre, swivel-typed cruciform, spiro-centred cruciform, have once attracted much attention.<sup>4</sup> However, these materials usually have a complex synthesis route and are difficult to crystallize. Furthermore, the electron delocalization between the conjugated branches is discontinued. They may be possibly more suitable for applications as highly luminescent materials.<sup>5</sup> To improve the molecule conjugation and crystal packing,  $\pi$ -conjugated planar molecules may be more preferable to develop new 3D organic semiconductors.

From the point view of molecule figure, the reported planar organic semiconductors can be roughly classified into linear, star and cruciform shapes, and the molecular shape can exert a drastic effect on the optoelectronic property.<sup>6</sup> Among them, linear molecules have been mostly focused. Linear organic semiconductors can easily adopt an edge-on orientation on the substrate and the direction of strong intermolecular interaction is parallel to the direction of carrier transport. This endows them with good FET properties. However, linear  $\pi$ -conjugated molecules usually self-assemble into a 2D electronic structure, such as herringbone or slipped  $\pi$ -stacks.<sup>1,7</sup> It is difficult for them to form a 3D electronic packing and only a few examples are

reported.<sup>2b,2c</sup> Though some star and cruciform-shaped  $\pi$ -conjugated molecules have been used in OFET devices, their crystal packing is seldom reported.<sup>8</sup> This is possibly due to their flexible structure, which may bring difficulty to crystallize.

5 Compared to the linear shape, star-shaped molecules have three conjugated arms which can interact with other arms of near molecules in the spatial structure. Therefore, star-shaped molecules with propeller structure would be more promising to form a 3D electronic packing. Kirchmeyer and co-workers once  
10 proposed a 3D lamellar structure of star-shaped oligothiophenes.<sup>8c</sup> However, due to the lack of some crystal structure proofs, the aggregate packing of star-shaped  $\pi$ -conjugated molecules is still puzzled and needs to be further studied.

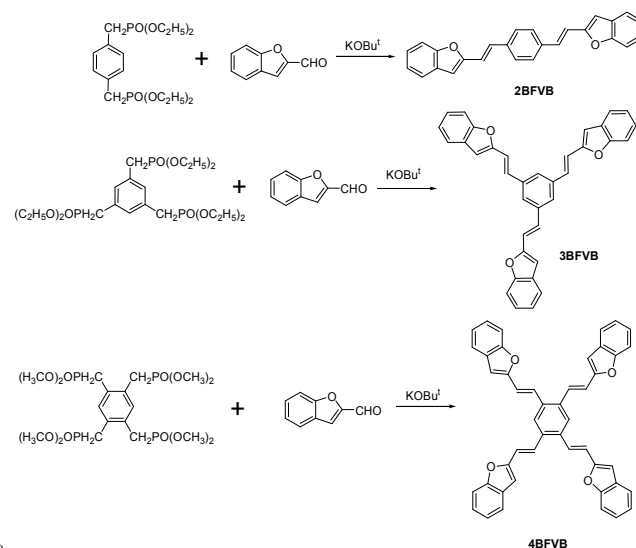
15 In comparison with thiophene, furan-based materials are scantily investigated in optoelectronic devices. Recently, furan-based semiconductors used in OFET and solar cell devices began to gain much attention.<sup>9,10</sup> Due to the differences in electronegativity, van der Waals radius and polarizability of  
20 oxygen from sulphur, replacing thiophene with furan often exerts remarkable effects on the material's electronic structure, solubility, crystal packing and optoelectronic properties. One outstanding character is that furan-based materials usually emit more efficiently.<sup>9a,9b,11</sup> Bendikov *et al.* reported that the solution  
25 emission efficiency of  $\alpha$ -oligothiophene was much higher than that of its corresponding  $\alpha$ -oligothiophene.<sup>11</sup> This was explained by the decreased heavy atom effect from sulphur to oxygen atom and the more molecular rigidity. In this paper, to explore new furan-based  
30  $\pi$ -conjugated materials and study the effect of multi-branched degree on the optoelectronic properties, compounds 1,4-bis[2-(benzofuran-2-yl)vinyl]benzene (**2BFVB**) with linear shape, 1,3,5-tris[2-(benzofuran-2-yl)vinyl]benzene (**3BFVB**) with star shape and 1,2,4,5-tetra[2-(benzofuran-2-yl)vinyl]benzene (**4BFVB**) with cruciform shape were synthesized and compared.  
35 Both **2BFVB** and **4BFVB** form a 2D electronic structure. However, **3BFVB** ( $\beta$ -phase) molecules pack into a 3D cofacial herringbone structure. The molecular shape exerts drastic effects on the solubility, polymorphism, crystal packing and optoelectronic properties.

## 40 Result and discussion

### Synthesis and characterization

All the compounds were easily prepared by one-step Horner-Emmons reaction (Scheme 1), similar to the thiophenylvinyl-substituted benzene derivatives.<sup>12</sup> **3BFVB** is soluble in THF and  
45 chloroform, and it can be purified by recrystallization from ethyl acetate. In contrast, the solubility of **2BFVB** and **4BFVB** is not good in ordinary solvents, but they are soluble in hot DMF and can be recrystallized from DMF carefully. All the molecules were characterized by high resolution mass spectra, nuclear magnetic resonance and X-ray single-crystal diffraction. The data were in good agreement with the proposed structure. The coupling constant of the vinylic protons in the <sup>1</sup>H NMR spectra ( $J=16$  or 16.4 Hz) clearly indicates the selective formation of *trans*-configured double bonds,<sup>13</sup> which is further verified by the  
50 corresponding crystal structure. Compared to **2BFVB** and **4BFVB**, the nuclear magnetic resonance signals of the vinylic

protons in **3BFVB** molecule are low-field shifted. This is due to the discontinued  $\pi$ -conjugation through *meta*-substitution which reinforces the deshielding effect of the C=C double bond.



60 **Scheme 1** Synthetic routes to **2BFVB**, **3BFVB** and **4BFVB**

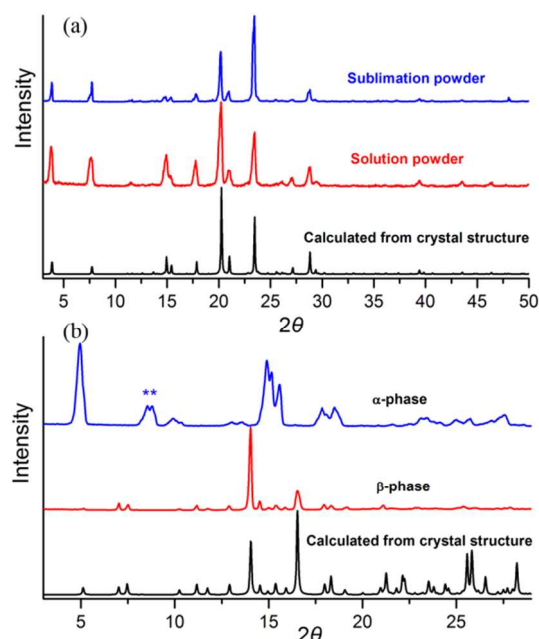


**Fig. 1** (a) XRD diffractograms of **2BFVB**. (b) XRD diffractograms of **3BFVB**.

65 The thermal properties of the three compounds were investigated by the thermogravimetric (TG) and differential scanning calorimetry (DSC) analyses (Fig. S1). **2BFVB** and **3BFVB** are thermally stable below 350 °C. In comparison, **4BFVB** starts to decompose at the melting point of 286 °C. There is no thermal transition for **2BFVB** solid before the melting point.  
70 In contrast, **3BFVB** and **4BFVB** exhibit one endothermic transition at 176 °C and 153 °C, respectively. The crystals of **4BFVB** were successfully grown by the vapour diffusion of the methanol (an anti-solvent) into a saturated DMF solution. The  
75 crystals of both **2BFVB** and **3BFVB**, which are suitable for a single-crystal X-ray diffraction, were grown by the physical

vapour transport method. As shown in Fig. 1a, the powder X-ray diffraction (XRD) pattern of **2BFVB** recrystallized from DMF is the same as that calculated from the crystal structure. However, a new thin-film phase was found during the vacuum-deposition of **2BFVB** onto Si/SiO<sub>2</sub> substrate (vide infra). Interestingly, **3BFVB** is more sensitive to the growing condition. The crystals grown by sublimation ( $\beta$ -phase) are yellow and stick-like, while the crystals from ethyl acetate ( $\alpha$ -phase) are pale-yellow and needle-like. The  $\beta$ -phase structure is determined by a single-crystal X-ray diffraction. However, the crystals from solution are not big enough for the single-crystal X-ray diffraction. The XRD analyses show that the diffraction pattern of **3BFVB** ( $\alpha$ -phase) is different from that of **3BFVB** ( $\beta$ -phase). As shown in Fig. 1b, the two obvious diffraction peaks of **3BFVB** ( $\alpha$ -phase) at  $2\theta = 8.55^\circ$  and  $8.79^\circ$  (marked with asterisks) are not present in the XRD pattern of **3BFVB** ( $\beta$ -phase). What is more interesting is that another new thin-film phase was also found during the vacuum-deposition of **3BFVB** onto octadecyltrichlorosilane-pretreated (OTS) Si/SiO<sub>2</sub> substrate (vide infra).

### Single-crystal structure

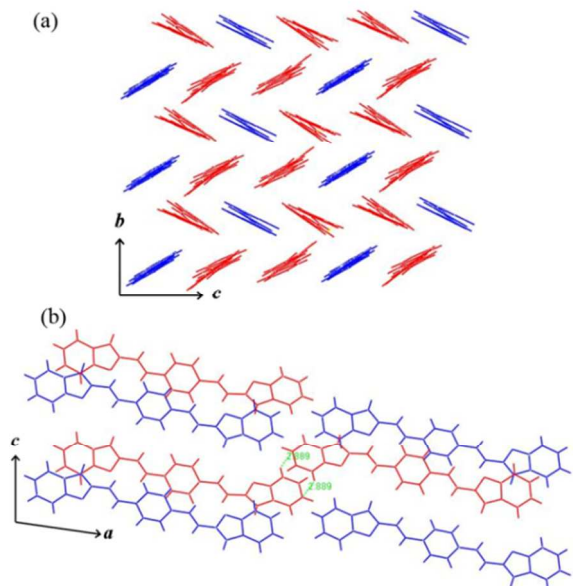
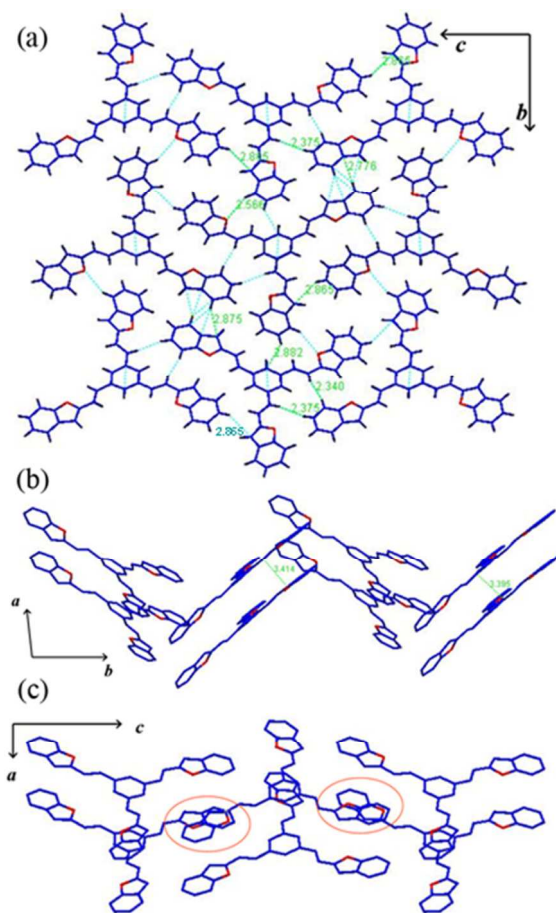


**Fig. 2** (a) Stacking image of **2BFVB** molecules in the  $bc$  plane. (b) Molecule packing in the  $ac$  plane. Red stands for the twisted conformation and blue for the planar conformation.

**2BFVB** compound crystallizes in the  $P2_1/c$  space group. There are two kinds of molecule geometries. One molecule has a little twisted configuration and the dihedral angle between the central benzene and the two peripheral benzofurans is  $2.12^\circ$  and  $10.82^\circ$ , respectively. The other molecule is more planar and has a 2-fold axis of symmetry. The dihedral angle is  $3.07^\circ$ . As shown in Fig. 2a, along the  $a$  axis, the molecules have their long axes parallel to each other and adopt a herringbone packing motif in the  $bc$  plane. Two-dimensional C-H $\cdots\pi$  interactions exist between the adjacent molecules. Along the  $b$  axis, the twisted (red colour) and planar molecules (blue colour) are arranged alternately to form a classical herringbone packing. There is nearly no face-to-face overlap between the adjacent parallel molecules for the centroid $\cdots$ centroid distance is  $7.576 \text{ \AA}$ . However, a cofacial

herringbone packing with slipped face-to-face interactions exist along the  $c$  axis as the centroid $\cdots$ centroid distance between adjacent parallel twisted and planar molecules is shortened to  $6.131 \text{ \AA}$ .<sup>1d</sup> Along the  $c$  axis, the adjacent two twisted molecules are oriented in the opposite direction. **2BFVB** molecules form a lamellar structure along the  $a$  axis (Fig. 2b). Interestingly, C-H $\cdots\pi$  interactions with a distance of  $2.889 \text{ \AA}$  exist between the twisted molecules in the adjacent layers. This is different from 4,4'-bis[2-(1-naphthyl)vinyl]benzene, which has a classical herringbone packing.<sup>14</sup> Overall, **2BFVB** belongs to a 2D semiconductor kind.



to-edge arrangements through C-H $\cdots\pi$  interactions (Fig. 3a and 3b). The C-H $\cdots$ C distances include 2.776, 2.875 and 2.882 Å, and the C-H $\cdots$ O distance is 2.566 Å. As shown in Fig. 3c, along the *c* axis, slipped  $\pi\cdots\pi$  interaction exists between the two arms of the adjacent molecules (labelled by red circles). The centroid $\cdots$ centroid distance between the two benzofuran rings is 5.818 Å and the shortest C $\cdots$ C distance is 3.769 Å. C-H $\cdots\pi$  interactions with a distance of 2.865 Å and H $\cdots$ H interactions with distances of 2.340 and 2.375 Å also exist in the direction of the *c* axis (Fig. 3a). Therefore **3BFVB** molecules form a 3D electronic packing.

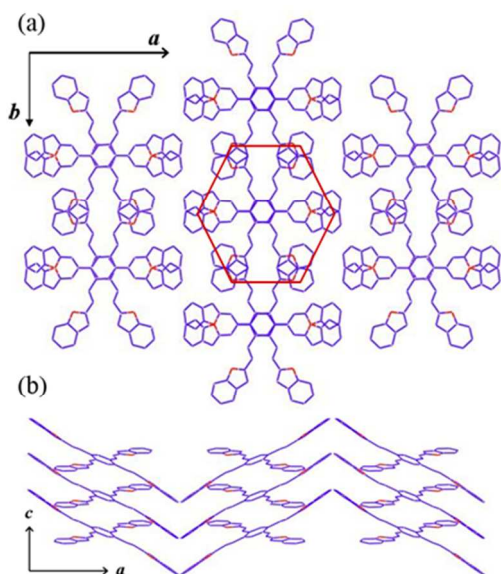


**Fig. 4** (a) Stacking image of **4BFVB** molecules in the *ab* plane. (b) Molecule packing in the *ac* plane.

**4BFVB** compound crystallizes in the *Pbcn* space group. There is a half symmetry-independent molecule per asymmetric unit. The dihedral angle between the central benzene and the peripheral benzofurans is 19.33° and 20.39°, respectively. As shown in Fig. 4a, the molecules pack into an inter-inserted hexagon packing structure along the direction of the *c* axis. However, the adjacent molecules are not parallel and the dihedral angle of the two benzene cores is 26.25°. The first molecule is parallel to the third one along the *c* axis. Every **4BFVB** molecule has four benzofuran arms. A pair of benzofuran rings interacts with the underground and overground benzofurans along the *c* axis mainly by  $\pi\cdots\pi$  interaction as the dihedral angle is only 7.03°. The centroid $\cdots$ centroid and shortest C $\cdots$ C distances are 4.459 and 3.325 Å, respectively. The other pair of benzofuran rings interacts with the adjacent upper and lower benzofurans along the *b* axis with a big dihedral angle of 22.38°. Though **4BFVB** molecules also adopt a zigzag packing along the *a* axis (Fig. 4b), the adjacent molecules adopt an end-to-end arrangement and the intermolecular interaction along the *a* axis is weak. Therefore, **4BFVB** also belongs to a 2D semiconductor kind.

### Photophysical properties

Optical properties of the three materials were characterized in THF solution and as crystalline solid, respectively. The absorption and emission properties are summarized in Table 1.

As shown in Fig. 5, it is clearly seen that the substitution degree exerts remarkable effects on the optical properties. As for the THF solution, the absorption maximum is 391 nm for **2BFVB**, 346 nm for **3BFVB** and 377 nm for **4BFVB**. The corresponding emission maximum is 453, 412 and 487 nm, respectively. The solid emission of the three materials ranges from 454 to 584 nm. Compared to **2BFVB** and **4BFVB**, both the absorption and emission spectra of **3BFVB** display a blue-shift feature. This is possibly attributed to the discontinued  $\pi$ -conjugation through *meta*-substitution.<sup>6b,15</sup> Another prominent character is that both the absorption and emission spectra of **2BFVB** and **3BFVB** solutions are vibronically structured and approximately mirror-symmetrical. In contrast, **4BFVB** solution displays a broad spectrum both in the absorption and in the emission. These observations indicate a greater molecular rigidity of **2BFVB** and **3BFVB** than **4BFVB**. In comparison with **4BFVB**, the smaller Stokes shifts in **2BFVB** and **3BFVB** solution spectra also indicate that **2BFVB** and **3BFVB** structures are more rigid.<sup>9b</sup>

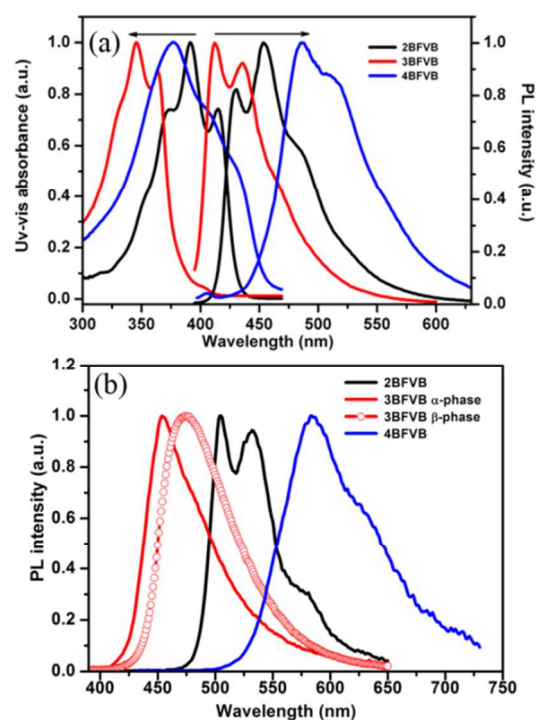


**Fig. 5** (a) Normalized optical absorption (UV/vis) and emission spectra in THF solution of the three materials. (b) The solid emission spectra. The emission spectra were obtained by exciting at 377 nm.

The fluorescence quantum yield ( $\Phi_f$ ) and photoluminescence decay dynamics of the three materials were also measured and the results are also shown in Table 1. **2BFVB** emits efficiently both in the solution and in the solid state. Though **2BFVB** molecule stacks into a herringbone-arranged H-aggregate in the crystalline solid, it does not suffer from an aggregation-caused quenching effect which was usually observed in the H-aggregates.<sup>14,16</sup> The quantum yield of **2BFVB** crystalline solid is as high as 76%, which ranks into the several highly luminescent H-aggregates.<sup>17</sup> The high emission efficiency of **2BFVB** crystals may be closely related to the two molecule geometries in the crystal structure. This two kinds of molecules alternately align along the herringbone stacking direction, which is similar to the reported

structure of 2-([1,1'-biphenyl]-4-yl)-5-(5-([1,1'-biphenyl]-4-yl)thiophen-2-yl)furan (**BPFT**).<sup>9b</sup> Theoretical analysis reveals that the high photoluminescence efficiency of **BPFT** originates from the symmetry breaking of the H-aggregate due to the two kinds of molecule geometries.<sup>18</sup> This may also explain the high emission efficiency of **2BFVB** crystalline solid. Both **3BFVB** and **4BFVB** display an aggregation-caused quenching behaviour and the solution emits more efficiently than the solid. For  $\pi$ -conjugated hydrocarbons, it has been studied that there is a correlation between the solution  $\Phi_F$  and the magnitude ( $A_\pi$ ) of the conjugation length.<sup>19</sup> The bigger the  $A_\pi$  value is, the higher the  $\Phi_F$  is. As for the three materials, the  $A_\pi$  value is in decreasing order from **2BFVB**, **4BFVB** to **3BFVB** as the *meta*-substitution disrupts the  $\pi$ -electron conjugation. Thus, **2BFVB** solution emits most efficiently.

**Table 1** Absorption and emission properties of **2BFVB**, **3BFVB** and **4BFVB** in  $10^{-5}$  M THF solution and in the solid state.

	Solution				Solid		
	$\lambda_{\text{abs}}$ (nm)	$\lambda_{\text{em}}^a$ (nm)	$\tau$ (ns)	$\Phi_F$	$\lambda_{\text{em}}^a$ (nm)	$\tau$ (ns)	$\Phi_F$
<b>2BFVB</b>	375 391 415	430 453 485	1.58	74%	504 532	4.42	76%
<b>3BFVB</b>	346 364	412 436	8.04	34%	454 ( $\alpha$ -phase) 474 ( $\beta$ -phase)	9.42 ( $\alpha$ -phase) 6.08 ( $\beta$ -phase)	16% ( $\alpha$ -phase) 22% ( $\beta$ -phase)
<b>4BFVB</b>	377 405	487 512	7.61	53%	584	0.84 (0.67) <sup>b</sup> 4.60 (0.33)	16%

<sup>a</sup> Excitation wavelength is 377 nm for all compounds. <sup>b</sup> Fractional contribution.

### Structural investigation on the thin films and OFET Property

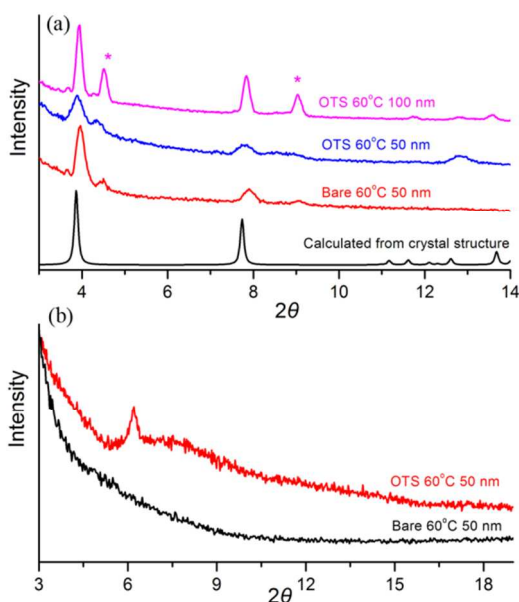


**Fig. 6** (a) XRD diffractograms of **2BFVB** films and the simulated powder pattern from crystal structure. (b) XRD diffractograms of **3BFVB** films. The films were deposited at 60 °C on bare and OTS-pretreated Si/SiO<sub>2</sub>.

Related to the substitution degree, the three compounds display different molecule packing. This would play a remarkable role in the vapour-deposited film morphology and, furthermore, the OFET performance. The morphology of the vapour-deposited films (about 50 nm) was investigated by XRD and atomic force microscopy (AFM) analyses. In order to improve the OFET performance, the surface pretreatment with OTS is usually used to reduce the surface energy between the semiconductor and the

The substitution degree also exerts a remarkable effect on the photoluminescence decay dynamics. The solution decay behaviours of the three materials are all single-exponential. However, the lifetime of **2BFVB** solution is only 1.58 ns, much shorter than those of **3BFVB** and **4BFVB**. This implies that the radiative decay process of **2BFVB** solution is rapid. As for the solid state, the decay dynamics of **2BFVB** and **3BFVB** also follow a single-exponential behaviour. However, the excited molecules in the **4BFVB** solid decay through two relaxation pathways. This implies that there may be two kinds of emissive species in the solid state, possibly related to the intermolecular  $\pi$ - $\pi$  interaction. The lifetimes in the  $\alpha$ -phase and  $\beta$ -phase of **3BFVB** are different, which may be attributed to the different molecule packing in the solid state.

SiO<sub>2</sub> interface. The substrate temperature has an effect on the film morphology. At high temperature, the semiconductor molecules can form more ordered packing and bigger crystalline grains, which will be beneficial to the carrier transport.<sup>1</sup> Therefore, the substrate temperature is set as 60 °C and 90 °C during device fabrication. For **4BFVB** is easy to decompose upon sublimation, the corresponding film morphology and OFET property were not studied.

As shown in Fig. 6a, the diffraction peaks in the **2BFVB** XRD patterns indicate the crystalline microstructure in the vacuum-deposited films both on bare and on OTS-pretreated Si/SiO<sub>2</sub>. In comparison with the simulated powder pattern based on the single-crystal structure, the film XRD peaks at  $2\theta = 3.94$  and  $7.84^\circ$  are assigned to (100) and (200) reflections. As can be seen from the crystal structure, the long axis of **2BFVB** molecule is nearly parallel to the crystallographic *a* axis. Therefore, the molecule should adopt an edge-on orientation on the substrate in (100) and (200) planes. This orientation is an ideal molecule arrangement to achieve high mobility because the dense stacking direction is consistent with the direction of current flow. **2BFVB** films also yield another discernable diffraction peaks at  $2\theta = 4.5$  and  $9.0^\circ$  (marked with asterisks). To elucidate this, a thicker film on OTS-pretreated Si/SiO<sub>2</sub> at about 100 nm was also deposited and characterized. Now the diffraction peaks at  $2\theta = 4.52$  and  $9.02^\circ$  are much clearer. However, these two peaks are not found in the simulated powder pattern from the single-crystal structure. Thus a new crystal phase would coexist in the deposited film. To get this new phase structure, we try to grow **2BFVB** crystals on OTS-pretreated Si/SiO<sub>2</sub> by the physical vapour transport method. However, the structure of the obtained crystals is the same as that of the previous crystals. Therefore this new crystal phase may be only a thin-film phase, not a bulk or single-crystal phase.<sup>1c</sup> For **3BFVB**, the XRD pattern of the film on bare Si/SiO<sub>2</sub> shows no

discernible reflection peaks (Fig. 6b), suggesting that the molecules were packed disorderly. On the contrary, the film on OTS-pretreated Si/SiO<sub>2</sub> shows a diffraction peak at  $2\theta = 6.20^\circ$ , indicating the improved molecule ordering after OTS pretreatment. Interestingly, this diffraction peak does not appear in the XRD pattern of either  $\alpha$ -phase or  $\beta$ -phase (Fig. 1b and Fig. 6b). Thus, the vacuum-deposited **3BFVB** film is also possibly a new thin-film phase.

Fig. 7 shows the AFM images of the thin films of **2BFVB** and **3BFVB**. The **2BFVB** films are mainly composed of plate-like grains, but the film continuity on OTS-pretreated Si/SiO<sub>2</sub> is much better. There are also some discernable block-like grains, which are much clearer in the 100 nm thick film. These two kinds of crystal forms in the AFM images are in accordance with the two sets of XRD patterns. The surface pretreatment exerts a more obvious effect on the **3BFVB** film morphology. The microstructure of the film on bare Si/SiO<sub>2</sub> is homogenous, displaying amorphous characteristics. However, the film on OTS-pretreated Si/SiO<sub>2</sub> is made up of long fiber-like grains.

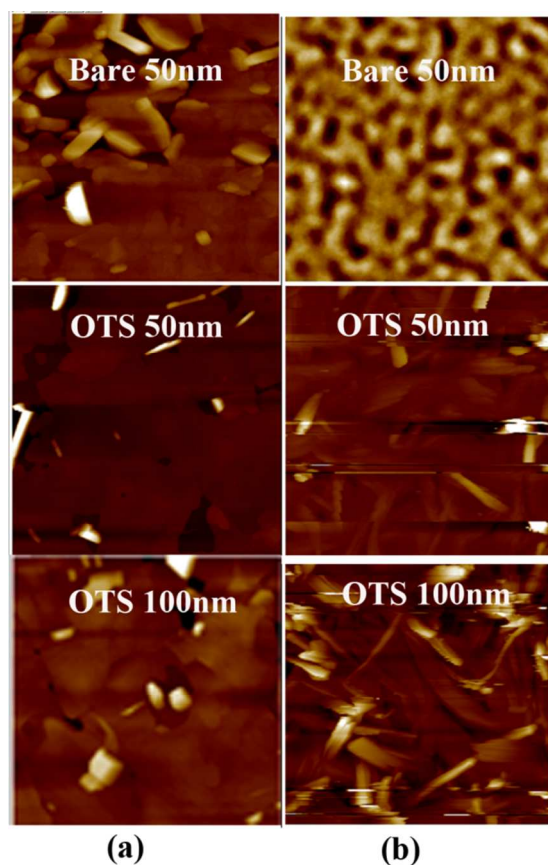


Fig. 7 AFM images of films deposited on bare and OTS-pretreated Si/SiO<sub>2</sub> at 60 °C (3  $\mu\text{m} \times 3 \mu\text{m}$ ): (a) **2BFVB**; (b) **3BFVB**.

OFET devices of **2BFVB** and **3BFVB** were fabricated using top-contact geometry. After sublimating the molecules onto the substrate, Gold was deposited as source and drain electrodes using a shadow mask with  $W/L = 60$ . The device performance was measured in air and the results are shown in Table 2. Both materials perform as p-type semiconductors. The hole mobility was extracted from the saturation regime of the transfer curve by using the classic equation describing field-effect transistor.

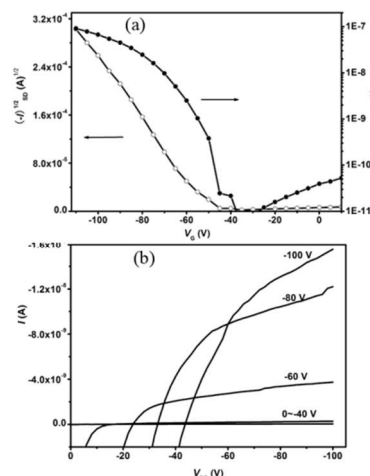


Fig. 8 OFET characteristics of **2BFVB** on OTS-pretreated substrate ( $T_{\text{sub}} = 60 \text{ }^\circ\text{C}$ ): (a) transfer characteristic at  $V_{\text{DS}} = -100 \text{ V}$ ; (b) output characteristic.

Table 2 The performance of OFETs based on **2BFVB** and **3BFVB**

	$T_{\text{sub}} (\text{ }^\circ\text{C})^a$	Si/SiO <sub>2</sub>	Mobility ( $\text{cm}^2 \text{ V}^{-1} \text{ s}^{-1}$ )	$I_{\text{on}}/I_{\text{off}}$ ratio
<b>2BFVB</b>	60	Bare	$1.8 \times 10^{-7}$	$10^2\text{-}10^3$
		OTS	$1.4 \times 10^{-4}$	$10^3\text{-}10^4$
<b>3BFVB</b>	60	OTS	$4.6 \times 10^{-4}$	$10^3\text{-}10^4$
		Bare	$1.2 \times 10^{-6}$	$10^2\text{-}10^3$
		OTS	$1.9 \times 10^{-6}$	$10^2\text{-}10^3$

<sup>a</sup> Substrate temperature.

As shown in Table 2, the OFET property of **2BFVB** is much better than those of **3BFVB** after OTS pretreatment. The typical field-effect transistor transfer and output characteristics of **2BFVB** on OTS-pretreated SiO<sub>2</sub> at 60 °C are presented in Fig. 8. The mobility was found to be  $1.4 \times 10^{-4} \text{ cm}^2 \text{ V}^{-1} \text{ s}^{-1}$  with an on/off current ratio of  $10^3\text{-}10^4$ . The performance is higher than that of devices fabricated on bare SiO<sub>2</sub> possibly for the improved film continuity (Fig. 7a). As we know, the extension of  $\pi$ -conjugation is an effective approach to get high carrier mobility for enhancing the intermolecular couplings.<sup>1d</sup> The low OFET performance of **2BFVB** is possibly due to the still short  $\pi$ -conjugation length. This can be clearly seen from the OFET performance of 1,4-bis[2-(1-naphthyl)vinyl]benzene and 4,4'-bis[2-(1-naphthyl)vinyl]biphenyl, whose molecular structure is similar to **2BFVB**. The  $\pi$ -conjugation of the latter molecule is longer and the carrier mobility increases from  $10^{-6} \text{ cm}^2 \text{ V}^{-1} \text{ s}^{-1}$  to  $10^{-3} \text{ cm}^2 \text{ V}^{-1} \text{ s}^{-1}$ .<sup>14</sup> As shown in Fig. 6, both **2BFVB** and **3BFVB** can form crystalline film on OTS-pretreated SiO<sub>2</sub> at 60 °C. However, the carrier-transport ability of **3BFVB** is much lower than that of **2BFVB**. There are possibly two main reasons. On the one hand, the  $\pi$ -conjugation degree of **3BFVB** molecule is lower than that of **2BFVB**. This could weaken the intermolecular couplings.<sup>1d</sup> On the other hand, **3BFVB** film is composed of 1D fiber-like grains. While **2BFVB** film is mainly composed of 2D lamellar grains. The carrier transport is more effectively in a 2D percolation network than a 1D one.<sup>3</sup> The OFET characteristics of **2BFVB** on OTS-pretreated SiO<sub>2</sub> at  $T_{\text{sub}} = 90 \text{ }^\circ\text{C}$  and **3BFVB** at  $T_{\text{sub}} = 60 \text{ }^\circ\text{C}$  are shown in Fig. S2 and S3.

Though the mobility of **3BFVB** is low, the performance of its film on bare Si/SiO<sub>2</sub> is near to that on OTS-pretreated Si/SiO<sub>2</sub>. In

other words, the carrier-transport ability of the amorphous film is nearly equal to that of the crystalline film. This implies that the careful control of molecular orientation during device fabrication, such as OTS pretreatment, may be not imperative. This could considerably simplify the fabrication of organic devices, which was considered as one of the notable advantages of 3D organic semiconductors.<sup>2c,4a</sup> Next we will aim to improve the carrier-transport ability of star-shaped planar molecules by increasing the  $\pi$ -conjugation degree of the single arm.

## 10 Experimental

### Chemicals and instruments

Benzofuran-2-carboxaldehyde and 1,4-bis(diethoxyphosphorylmethyl)benzene were purchased from J&K Scientific and used as received without further purification. 1,3,5-Tris(diethoxyphosphorylmethyl)benzene and 1,2,4,5-tetra(dimethoxyphosphorylmethyl)benzene were prepared according to the published procedure.<sup>6b</sup>

<sup>1</sup>H NMR and <sup>13</sup>C NMR spectra were recorded on a Bruker Avance 400 spectrometer. Elemental analyses were performed using a PerkinElmer 2400II analyzer. Absorption measurements were carried out on a TU-1800 spectrophotometer. Photoluminescence measurements and time-resolved emission decay behaviour were recorded on an Edinburgh Instruments FLS920. The absolute photoluminescence quantum efficiency ( $\Phi_F$ ) values of the solid and THF solution were determined on an Edinburgh Instruments FLS920 using an integrating sphere. High-resolution mass spectral analyses were carried out on a Bruker maXis UHR-TOF mass spectrometer. Thermogravimetric (TG) and differential scanning calorimetry (DSC) analyses were measured on a METTLER TOLEDO TGA/DSC 1 instrument, in a flowing nitrogen atmosphere and with a 10 °C min<sup>-1</sup> to 500 °C. For morphological characterization, the materials were deposited onto Si/SiO<sub>2</sub> wafers simultaneously with the FET devices. The AFM images were obtained by using a Dimension Icon instrument operating at ScanAsyst mode. The XRD investigations were carried out on a Bruker D8 advance or D8 Focus diffractometer equipped with Cu K $\alpha$  radiation ( $\lambda = 1.5406 \text{ \AA}$ ). Single-crystal X-ray diffraction measurements were conducted on an Oxford Diffraction Gemini E diffractometer. The structure was solved by direct method and refined by a full-matrix least-squares technique on  $F^2$  using SHELXL-97 programs.<sup>20</sup> CCDC-980249 (**2BFVB**), 980250 (**3BFVB**) and 980251 (**4BFVB**) contain the supplementary crystallographic data for this paper. These data can be obtained free of charge from the Cambridge Crystallographic Data Centre via [www.ccdc.cam.ac.uk/data\\_request/cif](http://www.ccdc.cam.ac.uk/data_request/cif).

OFET devices were fabricated in the top contact configuration. Gold electrodes were deposited using shadow masks with a width-to-length ratio ( $W/L$ ) of ca. 60/1. Organic semiconductors were deposited at a rate of 0.1  $\text{\AA s}^{-1}$  to about 50 nm under a pressure of about  $5.0 \times 10^{-4}$  Pa. OFET characteristics were obtained at room temperature in air on Keithley 4200 SCS.

### Synthesis

**1,4-Bis[2-(benzofuran-2-yl)vinyl]benzene (2BFVB).** At 0 °C, KOBu<sup>t</sup> (0.67g, 5.98 mmol) in THF (20 mL) was added dropwise into a mixture of 1,4-

bis(diethoxyphosphorylmethyl)benzene (0.54 g, 1.43 mmol) and benzofuran-2-aldehyde (0.50 g, 3.42 mmol) in THF (20 mL) under argon. The reaction mixture was stirred overnight at room temperature. After filtration, the filtrate was recrystallized from DMF to give yellow solid (0.24 g, yield 46 %). Mp: 298 °C. <sup>1</sup>H NMR (CDCl<sub>3</sub>, 400 MHz)  $\delta$ : 6.71 (s, 2H), 7.04 (d,  $J = 16.4$  Hz, 2H), 7.20-7.23 (m, 2H), 7.26-7.30 (m, 2H), 7.32 (d,  $J = 16.4$  Hz, 2H), 7.48 (d,  $J = 7.6$  Hz, 2H), 7.53-7.55 (m, 6H). <sup>13</sup>C NMR (CDCl<sub>3</sub>, 100.62 MHz)  $\delta$ : 105.63, 111.05, 116.67, 121.00, 123.09, 124.87, 127.28, 129.30, 129.82, 136.61, 155.12, 155.21. Elemental analysis calcd (%) for C<sub>26</sub>H<sub>18</sub>O<sub>2</sub>: C, 86.16; H, 5.01; found: C, 85.82; H, 5.11.

### **1,3,5-Tris[2-(benzofuran-2-yl)vinyl]benzene (3BFVB).**

**3BFVB** was prepared according to the same procedure as that for **2BFVB** from benzofuran-2-aldehyde (0.31 g, 2.12 mmol), 1,3,5-tris(diethoxyphosphorylmethyl)benzene (0.33 g, 0.62 mmol) and KOBu<sup>t</sup> (0.40 g, 3.57 mmol). The product was recrystallized from ethyl acetate to give pale yellow solid (0.14 g, yield 45%). Mp: 278 °C. <sup>1</sup>H NMR (CDCl<sub>3</sub>, 400 MHz)  $\delta$ : 6.74 (s, 3H), 7.12 (d,  $J = 16.4$  Hz, 3H), 7.21-7.25 (m, 3H), 7.29-7.33 (m, 3H), 7.37 (d,  $J = 16.4$  Hz, 3H), 7.51 (d,  $J = 8.0$  Hz, 3H), 7.56 (d,  $J = 7.6$  Hz, 3H), 7.62 (s, 3H). <sup>13</sup>C NMR (CDCl<sub>3</sub>, 100.62 MHz)  $\delta$ : 105.88, 111.11, 117.50, 121.09, 123.13, 124.74, 124.99, 129.25, 129.74, 137.75, 154.98, 155.16. MS:  $m/z$  calcd for C<sub>36</sub>H<sub>24</sub>O<sub>3</sub>: 505.1725 [M+H]<sup>+</sup>; found: 505.1875

### **1,2,4,5-Tetra[2-(benzofuran-2-yl)vinyl]benzene (4BFVB).**

**4BFVB** was prepared according to the same procedure as that for **2BFVB** from benzofuran-2-aldehyde (0.30 g, 2.46 mmol), 1,2,4,5-tetra(dimethoxyphosphorylmethyl)benzene (0.29 g, 0.51 mmol) and KOBu<sup>t</sup> (0.46 g, 4.11 mmol). DMF was used as the solvent. The product was recrystallized from DMF to give brown solid (0.19 g, yield 57.7 %). Mp: 286 °C (dec.). <sup>1</sup>H NMR (CDCl<sub>3</sub>, 400 MHz)  $\delta$ : 6.80 (s, 4H), 7.09 (d,  $J = 16.0$  Hz, 4H), 7.22-7.26 (m, 4H), 7.30-7.34 (m, 4H), 7.54-7.59 (m, 8H), 7.76 (d,  $J = 16.0$  Hz, 4H), 7.89 (s, 2H). <sup>13</sup>C NMR (CDCl<sub>3</sub>, 100.62 MHz)  $\delta$ : 106.02, 111.09, 119.31, 120.99, 123.01, 124.51, 124.93, 127.01, 129.10, 135.26, 154.99, 155.07. MS:  $m/z$  calcd for C<sub>46</sub>H<sub>30</sub>O<sub>4</sub>: 647.2144 [M+H]<sup>+</sup>; found: 647.2339.

## 95 Conclusion

In summary, three planar benzofuran-based molecules with linear, star and cruciform shape were synthesized. The molecular shape exerts drastic effects on the solubility, crystal packing, polymorphism and optoelectronic properties. **2BFVB** adopt a 2D herringbone packing motif and there are two kinds of molecular geometries. The crystal packing of **3BFVB** is more sensitive to the growing condition and three polymorphs were found. **3BFVB** ( $\beta$ -phase) molecules pack into a 3D cofacial herringbone structure. **4BFVB** forms an inter-inserted hexagon packing. **2BFVB** displays a high quantum yield both in the solution and in the crystalline solid. The two molecule geometries in the herringbone-arranged H-aggregate possibly result into the high emission efficiency of **2BFVB** solid. Both **2BFVB** and **3BFVB** display hole-transport ability. The performance of **3BFVB** amorphous film is near to that of its crystalline film, which will be helpful to simplify the device fabrication. This study would be helpful to investigate the effect of substitution degree on the optoelectronic properties and explore new 3D organic

semiconductors.

## Acknowledgements

This work was supported by the National Natural Science Foundation of China (21202061, 21171069), the Natural Science Foundation of Shandong Province of China (ZR2011EMQ007) and Open Research Project (KF1208) from State Key Laboratory of Crystal Materials (Shandong University).

## Notes and references

<sup>a</sup> School of Chemistry and Chemical Engineering, University of Jinan, Jinan, China. E-mail: chm\_lxy@ujn.edu.cn; chm\_sungx@ujn.edu.cn.

<sup>b</sup> State Key Laboratory of Crystal Materials, Shandong University, Jinan, China.

†Electronic Supplementary Information (ESI) available: TG and DSC curves. The transfer and output characteristics of 2BFVB and 3BFVB. See DOI: 10.1039/b000000x/

- (a) T. Okamoto, C. Mitsui, M. Yamagishi, K. Nakahara, J. Soeda, Y. Hirose, K. Miwa, H. Sato, A. Yamano, T. Matsushita, T. Uemura and J. Takeya, *Adv. Mater.*, 2013, **25**, 6392; (b) D. Khim, H. Han, K.-J. Baeg, J. Kim, S.-W. Kwak, D.-Y. Kim and Y.-Y. Noh, *Adv. Mater.*, 2013, **25**, 4302; (c) J. Mei, Y. Diao, A. L. Appleton, L. Fang and Z. Bao, *J. Am. Chem. Soc.*, 2013, **135**, 6724; (d) H. Dong, X. Fu, J. Liu, Z. Wang and W. Hu, *Adv. Mater.*, 2013, **25**, 6158; (f) L. Torsi, M. Magliulo, K. Manoli and G. Palazzo, *Chem. Soc. Rev.*, 2013, **42**, 8612.
- (a) G. Schwabegger, M. Ullah, M. Irimia-Vladu, M. Baumgartner, Y. Kanbur, R. Ahmed, P. Stadler, S. Bauer, N. S. Sariciftci, H. Sitter, *Synth. Met.*, 2011, **161**, 2058; (b) M. J. Kang, T. Yamamoto, S. Shinamura, E. Miyazaki and K. Takimiya, *Chem. Sci.*, 2010, **1**, 179; (c) H. Pang, F. Vilela, P. J. Skabara, J. J. W. McDouall, D. J. Crouch, T. D. Anthopoulos, D. D. C. Bradley, D. M. de Leeuw, P. N. Horton and M. B. Hursthouse, *Adv. Mater.*, 2007, **19**, 4438.
- T. Vehoff, B. Baumeier, A. Troisi and D. Andrienko, *J. Am. Chem. Soc.*, 2010, **132**, 11702.
- (a) J. Roncali, P. Leriche and A. Cravino, *Adv. Mater.*, 2007, **19**, 2045; (b) J. Ohshita, Y. Hatanaka, S. Matsui, T. Mizumo, Y. Kunugi, Y. Honsho, A. Saeki, S. Seki, J. Tibbelin, H. Ottosson and T. Takeuchi, *Dalton Trans.*, 2010, **39**, 9314; (c) T. P. I. Saragi, T. Fuhrmann-Lieker and J. Salbeck, *Adv. Funct. Mater.*, 2006, **16**, 966.
- (a) T. P. I. Saragi, T. Spehr, A. Siebert, T. Fuhrmann-Lieker and J. Salbeck, *Chem. Rev.*, 2007, **107**, 1011; (b) D. Ni, B. Zhao, T. Shi, S. Ma, G. Tu and H. Wu, *ACS Macro Lett.*, 2013, **2**, 621; (c) J. Pina, J. Seixas de Melo, H. D. Burrows, A. Bilge, T. Farrell, M. Forster and U. Scherf, *J. Phys. Chem. B*, 2006, **110**, 15100.
- (a) M. Seri, A. Marrocchi, D. Bagnis, R. Ponce, A. Taticchi, T. J. Marks and Antonio Facchetti, *Adv. Mater.*, 2011, **23**, 3827; (b) A. Winter, C. Friebe, M. D. Hager and U. S. Schubert, *Eur. J. Org. Chem.*, 2009, 801; (c) R. Y. C. Shin, P. Sonar, P. S. Siew, Z.-K. Chen and A. Sellinger, *J. Org. Chem.*, 2009, **74**, 329.
- M. Mas-Torrent and C. Rovira, *Chem. Rev.*, 2011, **111**, 4833.
- (a) A. L. Kanibolotsky, I. F. Perepichka and P. J. Skabara, *Chem. Soc. Rev.*, 2010, **39**, 2695; (b) X. Mu, W. Song, Y. Zhang, K. Ye, H. Zhang and Y. Wang, *Adv. Mater.*, 2010, **22**, 4905; (c) S. A. Ponomarenko, S. Kirchmeyer, A. Elschner, B.-H. Huisman, A. Karbach and D. Drechsler, *Adv. Funct. Mater.*, 2003, **13**, 591; (d) K. H. Kim, Z. Chi, M. J. Cho, J.-I. Jin, M. Y. Cho, S. J. Kim, J. Joo and D. H. Choi, *Chem. Mater.*, 2007, **19**, 4925; (e) M. Y. Cho, S. J. Kim, Y. D. Han, D. H. Park, K. H. Kim, D. H. Choi and J. Joo, *Adv. Funct. Mater.*, 2008, **18**, 2905; (f) Y. Sun, K. Xiao, Y. Liu, J. Wang, J. Pei, G. Yu and D. Zhu, *Adv. Funct. Mater.*, 2005, **15**, 818.
- (a) O. Gidron, A. Dadvand, E. W.-H. Sun, I. Chung, L. J. W. Shimon, M. Bendikov and D. F. Perepichka, *J. Mater. Chem. C*, 2013, **1**, 4358; (b) K. Oniwa, T. Kanagasekaran, T. Jin, Md. Akhtaruzzaman, Y. Yamamoto, H. Tamura, I. Hamada, H. Shimotani, N. Asao, S. Ikeda and K. Tanigaki, *J. Mater. Chem. C*, 2013, **1**, 4163; (c) C. Mallet, Y. Didane, T. Watanabe, N. Yoshimoto, M. Allain, C. Videlot-Ackermann and P. Frère, *ChemPlusChem*, 2013, **78**, 459; (d) Y. Li, P. Sonar, S. P. Singh, W. Zeng and M. S. Soh, *J. Mater. Chem.*, 2011, **21**, 10829; (e) C. Mitsui, J. Soeda, K. Miwa, H. Tsuji, J. Takeya and E. Nakamura, *J. Am. Chem. Soc.*, 2012, **134**, 5448; (f) O. Gidron, A. Dadvand, Y. Sheynin, M. Bendikov and D. F. Perepichka, *Chem. Commun.*, 2011, **47**, 1976.
- (a) J. C. Bijleveld, B. P. Karsten, S. G. J. Mathijssen, M. M. Wienk, D. M. de Leeuw and R. A. J. Janssen, *J. Mater. Chem.*, 2011, **21**, 1600; (b) P. Sonar, S. P. Singh, E. L. Williams, Y. Li, M. S. Soh and A. Dodabalapur, *J. Mater. Chem.*, 2012, **22**, 4425; (c) C. H. Woo, P. M. Beaujuge, T. W. Holcombe, O. P. Lee and J. M. J. Fréchet, *J. Am. Chem. Soc.*, 2010, **132**, 15547.
- O. Gidron, Y. Diskin-Posner and M. Bendikov, *J. Am. Chem. Soc.*, 2010, **132**, 2148.
- (a) C. Hadad, J. C. García-Martínez and J. Rodríguez-López, *J. Org. Chem.*, 2012, **77**, 6223; (b) J. C. García-Martínez, E. Diez-Barra and J. Rodríguez-López, *Curr. Org. Synth.*, 2008, **5**, 267.
- C. Romero-Nieto, S. Merino, J. Rodríguez-López and T. Baumgartner, *Chem. Eur. J.*, 2009, **15**, 4135.
- Y.-X. Li, J. Jia and X.-T. Tao, *CrystEngComm*, 2012, **14**, 2843.
- C. W. Lee, J. A. Seo, M. S. Gong and J. Y. Lee, *Chem. Eur. J.*, 2013, **19**, 1194.
- (a) J. Cornil, D. Beljonne, J.-P. Calbert and J.-L. Brédas, *Adv. Mater.*, 2001, **13**, 1053; (b) X. Zhang, J. P. Johnson, J. W. Kampf and A. J. Matzger, *Chem. Mater.*, 2006, **18**, 3470.
- (a) J. Gierschner, L. Lüer, B. Milián-Medina, D. Oelkrug and H.-J. Egelhaaf, *J. Phys. Chem. Lett.*, 2013, **4**, 2686; (b) R. Kabe, H. Nakanotani, T. Sakanoue, M. Yahiro and C. Adachi, *Adv. Mater.*, 2009, **21**, 4034; (c) S.-J. Yoon, J. W. Chung, J. Gierschner, K. S. Kim, M.-G. Choi, D. Kim and S. Y. Park, *J. Am. Chem. Soc.*, 2010, **132**, 13675; (d) C. C. Wu, M. C. DeLong, Z. V. Vardeny and J. P. Ferraris, *Synth. Met.*, 2003, **137**, 939.
- H. Tamura, I. Hamada, H. Shang, K. Oniwa, Md. Akhtaruzzaman, T. Jin, N. Asao, Y. Yamamoto, T. Kanagasekaran, H. Shimotani, S. Ikeda and K. Tanigaki, *J. Phys. Chem. C*, 2013, **117**, 8072.
- (a) Y. Yamaguchi, Y. Matsubara, T. Ochi, T. Wakamiya and Z.-i. Yoshida, *J. Am. Chem. Soc.*, 2008, **130**, 13867; (b) S. Samori, S. Tojo, M. Fujitsuka, T. Ryhding, A. G. Fix, B. M. Armstrong, M. M. Haley and T. Majima, *J. Org. Chem.*, 2009, **74**, 3776.
- (a) G. M. Sheldrick, *SHELXL-97*, University of Gottingen, Gottingen, Germany, 1997; (b) O. V. Dolomanov, L. J. Bourhis, R. J. Gildea, J. A. K. Howard and H. Puschmann, *J. Appl. Cryst.*, 2009, **42**, 339.